Journal of the Australian Ceramic Society (2024) 60:629–642
https://doi.org/10.1007/s41779-024-01003-z

RESEARCH

# A spectroscopic study on the effect of acid concentration on the physicochemical properties of calcined halloysite nanotubes

**Meryem Türkay Aytekin Aydın**[1]

Received: 11 September 2023 / Revised: 10 January 2024 / Accepted: 9 February 2024 / Published online: 20 February 2024


## Abstract

Halloysite nanotubes a naturally occurring type of clay with unique properties. This research intends to investigate of the effects of hydrochloric acid treatment on the physicochemical and pore properties of halloysite nanotubes. X-ray diffraction (XRD), field emission scanning electron microscopy (SEM), Fourier-transform infrared (FT-IR) spectroscopy, the nitrogen adsorption-desorption isotherm (BET), thermogravimetric analyses (TGA-DTA) and X-ray photoelectron spectroscopy (XPS) were used to analyze the structure of natural, calcined, and acid-treated calcined halloysite nanotubes. From the analysis of XRD, SEM, FT-IR, BET, and TGA-DTA, it was possible to infer that activation with HCl on the calcined nanotubes allowed for an increase in the specific surface area and the volume of pores while maintaining the tubular structure of these materials. Because the samples' tubular structure was preserved, the study's goal was to evaluate the effects of acid treatment on calcined halloysite nanotubes for use as potential adsorbents. The influence of treatment with hydrochloric acid on the structure of halloysite nanotubes calcinated at different temperatures was investigated using a surface sensitive XPS method.

**Keywords** Halloysite · Hydrochloric acid · Characterization · FT-IR Calcination

## Introduction

Halloysite is a naturally occurring clay mineral that is physically and chemically analogous to kaolinite, dickite, or nacrite but differs in that it has a hollow microtubular structure rather than a stacked plate-like structure. Halloysite principally occurs in two different morphologies as hydrated form and anhydrous form [1]. Contrary to kaolinite, it is thought that the cause of this is the presence of water in the interlayer space [1–3]. Halloysite can be found in nature as tubular, plate, or spherical minerals due to the variations in geological formation, location, and crystallization mechanisms. The most intriguing of these various morphologies typically has a tubular form. Due to their hollow tubular structure, nanoscale diameter, specialized surface area, and unique surface properties, halloysite nanotubes have garnered a lot of attention Numerous nations, including China, New Zealand, Japan, South Korea, and Turkey, have abundant natural deposits of halloysite, which is easily and cheaply mined [2, 4, 5]. Tetrahedral Si − O and octahedral Al − O layers make up the two-layered aluminosilicate structure of halloysite, and these two layers are separated from one another by a monolayer of interlayer water molecules [2, 6]. As halloysite is a layer-structured mineral, it has two main groups, the hydrated form (with an interlayer spacing of 10 Å) with the formula $Al_2Si_2O_5(OH)_4.2H_2O$ and the anhydrous form (with an interlayer spacing of 7 Å) with the formula $Al_2Si_2O_5(OH)_4$ [1, 2, 4, 7]. The formation of the tubular structure in halloysite is actually the result of atomic scale stresses in the unit cell of the mineral. There are two types of sheet in the crystal structure of halloysite, tetrahedral (a = 5.02 Å, b = 9.164 Å) and octahedral (a = 5.066 Å, b = 8.655 Å) sheets [2]. These sheets are composed of different elements, including silicon (Si), aluminium (Al) and oxygen (O), and have different sizes and geometries. Typically, halloysite nanotubes are between 0.2 and 3 μm in length, with an outer diameter between 30 and 190 nm and an inner diameter between 10 and 100 nm [2, 4, 8, 9]. Halloysite and halloysite-based nanomaterials are widely used due to their tubular structure, unique surface properties,

✉ Meryem Türkay Aytekin Aydın
maytekin@eskisehir.edu.tr

[1] Science Faculty, Department of Physics, Eskişehir Technical University, Eskişehir 26470, Turkey

abundance in many countries, and economic viability. The uses for halloysite are numerous and diverse [2, 5]. Halloysite has been widely used for a variety of applications, such as antibacterial [10–13], drug delivery [14–18], enviromental and biomedical [19–21], energy storage [22–25] and adsorbent [26–29] uses because of its non-hazardous nature, ease of accessibility, hollow tubular structure, and large surface area. Furthermore, halloysite nanotubes have been applied in catalytic and technological applications in addition to being widely used in numerous fields of materials science and nanotechnology [30–35]. Recently, the effect of the acid treatment of halloysite has received special attention from many researchers [36–40]. Acid treatment is known an effective chemical procedure for the improvement of the surface area and catalytic properties of clay minerals [41, 42]. The use of different acids to treat clay minerals has been the subject of numerous studies [39–43]. The objective of the current study is to investigate the physicochemical behaviors of naturally occurring and hydrochloric acid-treated calcined halloysite nanotubes with respect to calcination temperature and acid concentration. The process of preparing calcined halloysite involves several important steps to ensure that the raw material is well-prepared for the subsequent calcination process. Calcination typically involves heating the prepared material at specific temperatures in a controlled atmosphere to drive off volatile components, water and other impurities. The calcination process transforms the raw material into calcined halloysite with altered properties, which can be used for a variety of industrial and scientific applications, such as catalyst supports, adsorbents, and reinforcing fillers in polymers. The effects of low concentrations of acid treatment after calcining at two different temperatures on the structure, morphology, and pore characteristics of halloysite nanotubes were examined using the proper analysis techniques. After being calcined at 250 and 600 ˚C, halloysite nanotubes were treated to 0.5 M, 1 M, and 2 M concentrations of hydrochloric acid. Reduced acid concentrations were used to limit the degree of chemical modification and prevent the nanotubes from dissolving too much. To control the hydrochloric acid's impact on the substances' tubular structure, the acid's concentration has been changed. The acid treatment and calcination processes used can provide significant information on the structure, morphology and pore characteristics of halloysite nanotubes, which are critical for various applications. The methods used in this study are beneficial in tailoring the nanotubes for specific applications while maintaining their structural integrity. It's important to note that maintaining the tubular structure may be desirable in certain applications, so the choice of treatment conditions should align with the intended use of the nanotubes. Overall, a thorough characterization and analysis of the halloysite nanotubes after different treatment conditions are essential for gaining a comprehensive understanding of how these treatments affect their physical characteristics for making informed decisions about their use and for optimizing their performance in various applications.

## Experimental procedure

### Synthesis of treated halloysite nanotubes

Halloysite nanotubes (HNTs) were obtained from Eczacıbasi Esan Co Ltd., Turkey. All of the chemicals used for the synthesis and spectroscopic studies were purchased from Sigma-Aldrich Chemie GmbH. The chemical composition of raw halloysite is given as follows: $SiO_2$ 43.30%, $Al_2O_3$ 38.40%, $Fe_2O_3$ 0.80%, $TiO_2$ 0.10%, CaO 0.08%, MgO 0.12%, $Na_2O$ 0.27%, $K_2O$ 0.12%, LOI 16.81%. The calcination halloysite preparation process was used in the present study. Halloysite was first wet milled using a laboratory jar mill and the slurry was screened with a 45-micron mesh. After grinding the raw materials, the slurry was dried at 100 ˚C for 24 h. For granulation of the dried powders, they were moistened by spraying water on them. The granules formed were passed through 250-micron sieves to collect between them. After granulation, the powders were calcined at 250 and 600 ˚C with a heating cycle of 10 ˚C/min for 2 h and then left to cool to room temperature in a desiccator. The outlines of the specific process of preparing calcined halloysite are wet milling, sieving, drying and granulation are steps that help prepare the raw material for calcination. The calcination process itself, conducted at two different temperatures, is crucial for altering the properties of halloysite according to the study's objectives. The overall process aims to create calcined halloysite with controlled properties for further experimentation or application in various fields. The natural halloysite powder was first calcined in a programed, temperature-controlled muffle furnace at two different temperatures (250 and 600 ˚C) for 2 h and then left to cool to room temperature in a desiccator. The calcined halloysite nanotubes were named C1HNT (at 250 ˚C 2 h) and C2HNT (at 600 ˚C 2 h). HNT is the name given to untreated natural halloysite nanotube. At room temperature, 10 g of the precalcined halloysite powder were added to 100 mL of a hydrochloric acid solution of various concentrations (0.5 M, 1 M, and 2 M). The obtained product was stirred for 2 h, and then was filtered, washed by distilled water until it reached a pH ≈ 6.0, and dried in an oven at 100 ˚C. The filtered product is washed with distilled water until the pH of the product is approximately 6.0. This step is crucial as it helps to remove any residual chemicals, impurities or acidic or alkaline substances. A pH of 6.0 indicates a slightly acidic solution, which is the desired condition for the final product.

Halloysite nanotubes treated with 0.5 M, 1 M, and 2 M HCl solutions after being calcined at 250 ˚C were named C1HNT0.5, C1HNT1 and C1HNT2, respectively. Additionally, halloysite nanotubes treated with 0.5 M, 1 M, and 2 M HCl solutions after being calcined at 600 ˚C were named C2HNT0.5, C2HNT1 and C2HNT2, respectively.

### Characterization methods

The characterization of the natural, calcined halloysite, and acid-treated calcined halloysite nanotubes was done using X-ray diffraction (XRD), scanning electron microscopy (SEM), Fourier transformed infrared spectroscopy (FT-IR), nitrogen adsorption and desorption (BET), and thermal analysis (TGA-DTA) methods. The X-ray diffraction patterns were obtained at room temperature using a BRUKER D8 Advance powder diffractometer with $CuK_{\alpha}$ target at 40 kV and 40 mA in the range of $5^{\circ} \leqslant 2\theta \leqslant 80^{\circ}$. The morphology of the nanotubes was evaluated with ZEISS Ultraplus model field emission scanning electron microscopy (SEM).

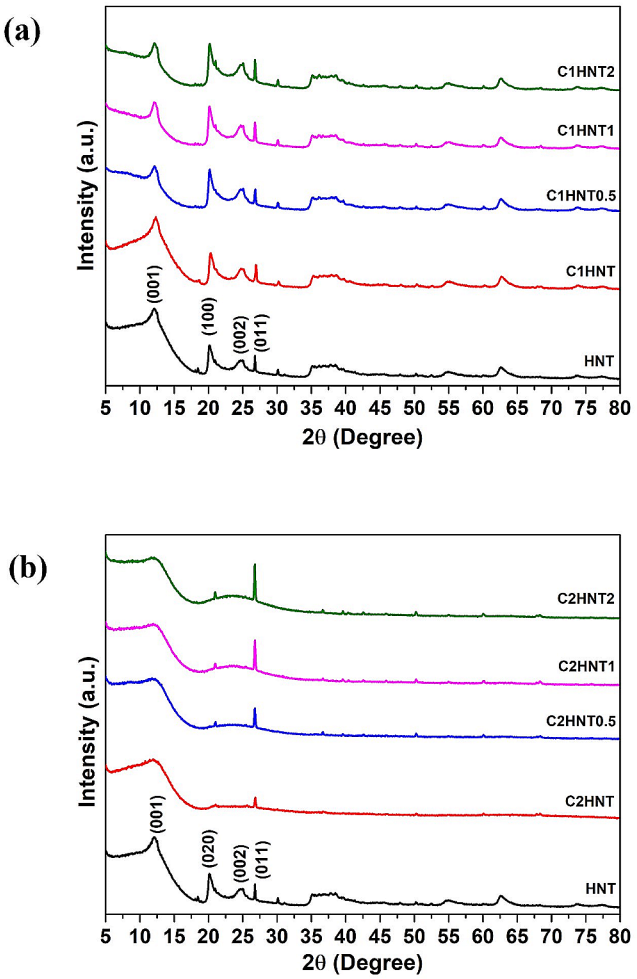


**Fig. 1** XRD patterns of **(a)** HNT, C1HNT, C1HNTC0.5, C1HNT1, C1HNT2, **(b)** HNT, C2HNT, C2HNT0.5, C2HNT1 and C2HNT2

Prior to examination, the samples were coated with gold using a sputter coater to prevent charging on the surface. The FT-IR spectra of the samples were recorded in the range of 4000 to 400 $cm^{-1}$ using a Bruker Optics IFS 66v/s FT-IR spectrometer at a resolution of 2 $cm^{-1}$ in vacuum. The pellets were prepared by mixing 1 mg of sample powder with 100 mg of KBr and drying them at 70 ℃ for 24 h before used. Using a Micromeritics Tristar 3020 surface area and pore analyzer, specific surface areas and pore size distributions of samples were determined by nitrogen adsorption at 77 K using the Brunauer Emmett-Teller (BET) method and the Barrett-Joyner-Halenda (BJH) method, respectively. Thermal gravimetric analysis (TG–DTA) was carried out with a Hitachi Hi-Tech STA7200 TGA analyzer system. The thermal analysis was carried out over the temperature range from room temperature to 800 ℃ with a 1 ℃/min heating rate under nitrogen flow. The XPS measurements were performed using a KRATOS ES300 spectrometer. The system is equipped with a non-monochromatic Mg Kα X-ray source.

## Results and discussion

### X-ray diffraction analysis

There were no appreciable differences found in the XRD patterns of the calcined and acid-treated calcined products compared to those previously reported for halloysite (7 Å). The dehydrated state and tubular structure of the halloysite nanotube (7 Å) are confirmed by the.

diffraction angles seen at $2\theta = 12.09^{\circ}$, $20.24^{\circ}$ and $24.85^{\circ}$ in agreement with the information provided by other researchers. The absence of the peak at $2\theta = 8.8^{\circ}$ in the XRD patterns of the products provides additional evidence of the dehydrated state [15, 16]. As shown in Fig. 1, the observed characteristic reflection 2θ values and corresponding planes at 12° (001), 20° (100), 25° (002), 35° (110), 55° (210) and 63° (300) are consistent with the earlier report of halloysite-7 Å (JCPDS card no. 29-1487) [16, 44]. After annealing temperature 600 ˚C, the XRD pattern have displayed noisy and the majority of the characteristic peaks of halloysite nanotube disappeared (Fig. 1). At the annealing temperature of 600 ˚C, a broad diffraction peak is observed in the range of 25–30˚ (2θ). The broad diffraction peak, identified as minor quartz, is probably due to the progressive amorphisation of the halloysite nanotube structure [43–46]. This behavior is often attributed to dehydroxylation, a process where hydroxyl groups (OH) are released from the material's structure at elevated temperatures. Halloysite is a natural mineral known for its tubular structure and the presence of hydroxyl

groups on its surface. At higher temperatures, particularly around 600 ˚C, these hydroxyl groups can start to dehydroxylate, leading to the loss of these characteristic peaks in the spectrum. These hydroxyl groups are often associated with the crystal lattice of the mineral, and the dehydroxylation process somewhat alters the original crystalline structure [46]. These findings affirm that halloysite nanotube is amorphous at temperature 600 ˚C [45–48]. The XRD patterns of the acid-treated halloysite nanotubes resemble those of those calcined at two different temperatures (Fig. 1).

As the concentration of hydrochloric (HCl) acid increased, there was no noticeably different peak in the characteristic peaks of calcined halloysite nanotubes. However, at the annealing temperature of 600 ˚C, a broad diffraction peak was observed in the range of 25–30˚ (2θ), with little increase in intensity with increasing hydrochloric acid concentration [45–48]. This obtained result is most likely due to the structure's progressive amorphization. The current XRD results strongly support the fact that the crystal structure is maintained after the acid treatment. The obtained results are consistent with similar studies [45–49].

## Scanning electron microscopy

The cylindrical tubular structures are visible in the SEM images of the naturally occurring, calcined, and acid-treated calcined halloysite nanotubes (Fig. 2). It is important to note that despite being subjected to acid treatment, nanotubes' tubular structures remained unchanged, and agglomerates were discernible at higher concentrations. These findings have revealed that.

the tubular structure of halloysite nanotube is preserved very well during acid-treatment even after increasing of the acid concentration [46, 49]. The physical characteristics of halloysite nanotubes become increasingly apparent as the acid concentration rises. The original tubular structures of the acid-treated samples are clearly visible, whereas samples calcined at 600 ˚C show more adhered and broken nanotubes (Fig. 2f-i). Additionally, the agglomerates in the samples calcined at 600 ˚C become apparent as the acid concentration is raised. The presence of adhered and broken nanotubes in the samples calcined at 600 ˚C indicates that this high-temperature treatment has a more pronounced impact on the nanotube structure. The sample calcined at 600 ˚C also give a tubular morphology, although the obtained tubes are damaged (Fig. 2f–i). This suggests that while the high temperature of 600 ˚C causes some structural damage to the halloysite nanotubes, it doesn't completely destroy their tubular shape. The damaged tubes may still have some degree of integrity left, albeit with alterations or defects. The results of the XRD analysis support the as-obtained findings.

## FT-IR spectroscopic analysis

Fourier transform infrared spectroscopy (FT-IR) is widely used in the field of geology and mineralogy because it provides valuable information about the molecular composition and structure of minerals [50–52]. Fourier transform infrared spectroscopy is a valuable analytical method for studying clay minerals, including water analysis. It is common practice to demonstrate the presence of the hydroxyl stretching and bending vibration frequencies in the halloysite's infrared spectrum in order to obtain spectroscopic information about water in the structure. FT-IR spectroscopy is a powerful analytical technique that provides information about the functional groups and chemical bonds present in a sample [53]. FT-IR spectra display absorption bands at characteristic wavenumbers that correspond to the vibrational modes of chemical bonds in the sample. By analyzing the positions and intensities of these absorption bands, it is possible to identify the functional groups that are present. Different types of chemical bonds can be identified based on the position of the absorption bands. Changes in the FT-IR spectrum can indicate alterations in the material's structure. It's also important to compare the spectrum of the sample with reference spectra or known standards to make accurate structural identifications. The appearance or disappearance of peaks or shifts in absorption bands when comparing the FT-IR spectra of two samples may indicate structural changes or chemical transformations. The typical vibration modes of natural halloysite were visible in the.

FT-IR spectrum (Fig. 3). The observed bands at around 3695 and 3623 $cm^{-1}$ are ascribed to the stretching vibration frequencies of the inner surface hydroxyl groups and inner hydroxyl groups, respectively [45, 47–49]. Furthermore, the broad band at about 3500 $cm^{-1}$ and the weak band at 1640 $cm^{-1}$ are attributed to the physically adsorbed water's O-H stretching and deformation, respectively [45, 47–49].

Specifically, the vibration modes of the skeletal bonds were seen below 1500 $cm^{-1}$. The bands at near 1120 and 1030 $cm^{-1}$ are due to Si–O stretching vibration and the Si–O–Si in-plane stretching vibration, respectively [45, 47–49]. The peak at 913 $cm^{-1}$ is ascribed to Al–O–H the inner-surface hydroxyl group. The peaks observed at 756 and 689 $cm^{-1}$ are due to Si–O stretching. The three peaks at 540, 468, and 433 $cm^{-1}$ are observed due to the deformation of Al–O–Si, Si–O–Si, and Si–O, respectively [45, 47–49]. There were no observed significant changes in the infrared spectra up to 600 ˚C (Fig. 3). The structural changes were observed in the infrared spectrum of halloysite nanotubes following calcination at 600 ˚C. In the case of calcination at 600 ˚C, the majority of the halloysite nanotubes' characteristic vibration peaks disappeared or broadened. The relationship between infrared vibrations and the amorphous

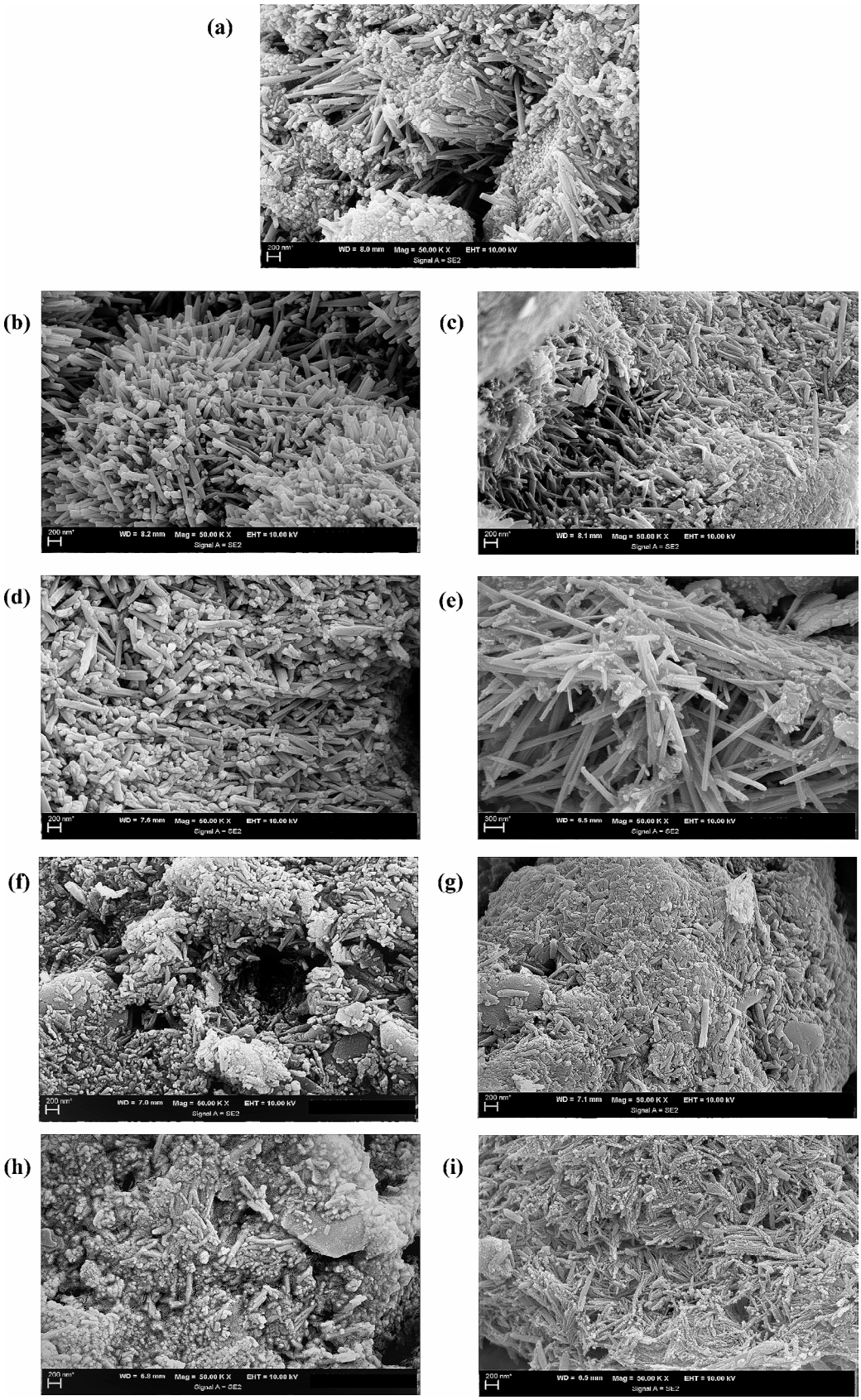


**Fig. 2** Scanning electron micrographs of **(a)** HNT, **(b)** C1HNT, **(c)** C1HNTC0.5, **(d)** C1HNT1, **(e)** C1HNT2, **(f)** C2HNT, **(g)** C2HNT0.5, **(h)** C2HNT1 and **(i)** C2HNT2

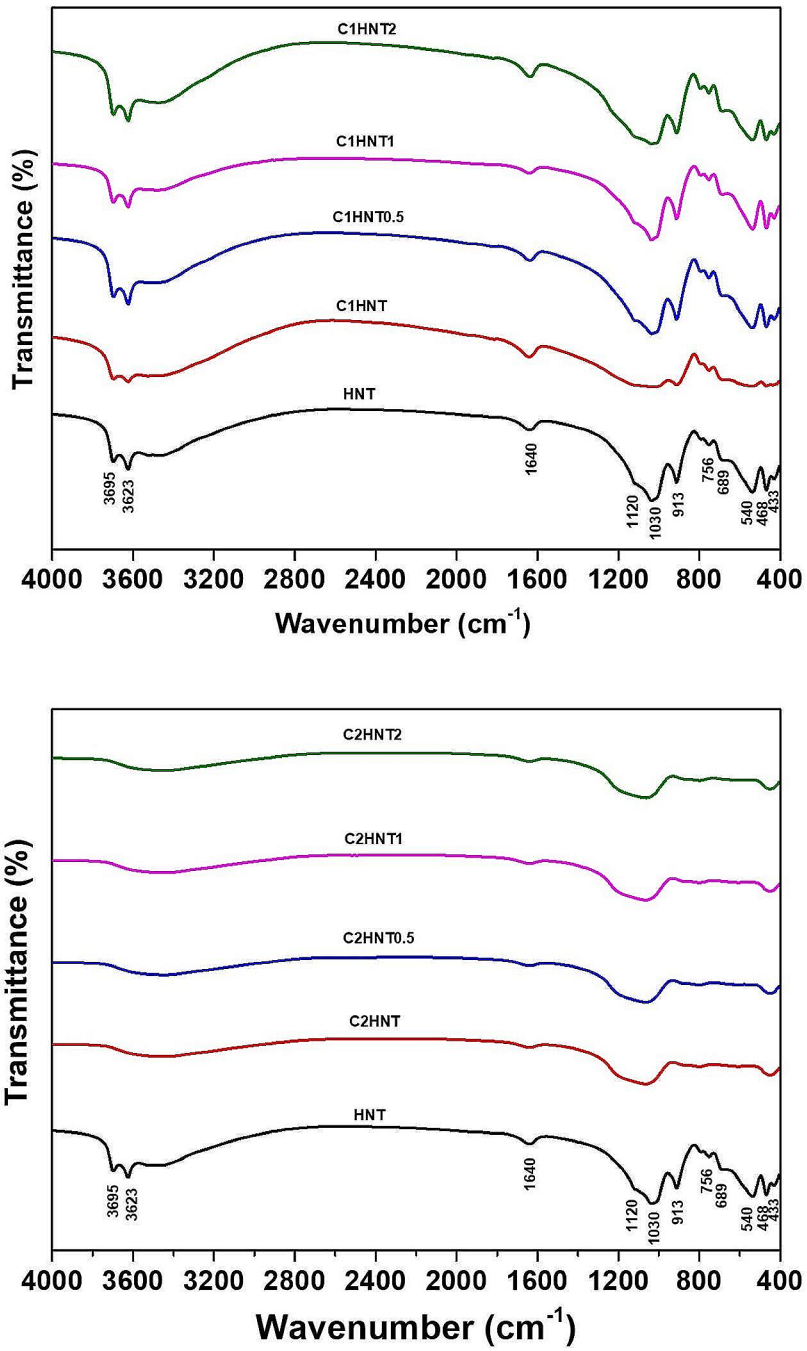


**Fig. 3** Infrared spectra of **(a)** HNT, C1HNT, C1HNTC0.5, C1HNT1, C1HNT2, **(b)** HNT, C2HNT, C2HNT0.5, C2HNT1 and C2HNT2

character in halloysite nanotubes lies in the observed changes in the infrared spectrum following calcination at 600 ˚C. The observed changes in the infrared spectrum suggest that the calcination at 600 ˚C has a profound impact on the molecular structure of halloysite nanotubes, leading to an almost amorphous and structurally disordered state [45, 47, 48]. The disappearance or broadening of characteristic vibrational peaks in the infrared spectrum is an indication that the characteristic vibrational modes associated with crystalline structures are no longer present or are more poorly defined. The disappearance or broadening of peaks in the infrared spectrum indicates the amorphisation of halloysite nanotubes and provides valuable information about the structural disorder induced by the calcination process [48]. In comparison to the infrared spectrum of an untreated halloysite nanotube, the calcined sample at 600 ˚C exhibits

a broad OH vibration band at about 3460 $cm^{-1}$. At 600 ˚C, halloysite is thought to be dehydroxylated, which causes this behavior. In particular, the disappearance of the characteristic bands in the region 3700 – 3500 $cm^{-1}$ confirms the structure's dehydroxylation [45, 47–49]. After being calcined at 250 ˚C and treated with acid, no discernible change was noticed when the concentration of acid was raised in the infrared spectra. The examination of the infrared spectra of the acid treated samples at 600 ˚C reveal many bands are lost and is observed only one very broad OH vibration band at about 3460 $cm^{-1}$ compared to those of untreated halloysite nanotubes. On the other hand, the broadening of characteristic vibration peaks after calcination at 600 ˚C indicates a significant change in the material's structure, moving from an ordered crystalline arrangement to a more disordered and amorphous state (Fig. 3). The stretching vibrations of Si–O and Al–O are usually observed in the range of 1200 – 800 $cm^{-1}$ [53]. The bending vibrations of Si–O and Al–O bonds are commonly found in the range of 400–700 $cm^{-1}$ [53]. The disappearance or broadening of these peaks in the infrared spectrum after calcination at 600 ˚C probably indicates a change in the crystal structure due to processes such as amorphization or dehydroxylation [45–48]. The change of the crystal structure due to dehydroxylation or amorphization may result in the disappearance or broadening of Si–O and Al–O vibrational modes. Treatment with HCl acid was first explored with a 0.5 M solution, but no modifications were observed in the spectroscopic properties of the calcined halloysite nanotubes at 600 ˚C. Even with the 2 M concentration, the infrared spectra of the samples did not observe significant variations with respect to the calcined halloysite nanotubes at 600 ˚C. No differences were observed in the infrared spectra, all of them showing the presence of this amorphous phase at 600 ˚C. The results of the infrared spectra suggest that despite the use of acid treatment, the concentrations used were not strong enough to cause significant changes in the absorption peaks of the halloysite nanotubes calcined at 250 and 600 ˚C [46, 47]. Based on the infrared spectroscopic data, it can be concluded that the acid treatment did not induce major changes in the structure or composition of the sample [46, 47, 49]. This suggests that the acid treatment process, under these conditions, does not significantly alter the chemical composition or structural integrity of the nanotubes as evidenced by the infrared spectra. The preservation of the nanotube structure can be important in a variety of applications where the specific structure and properties of the nanotubes are desired.

## Nitrogen adsorption-desorption and BET analysis

The nitrogen adsorption and desorption analyses of natural, calcined and calcined acid-treated halloysite nanotubes have been used to investigate the effect of the acid treatment process on the surface area and adsorption pore volume. The results show that the samples belong to isothermal type II with an H3 hysteresis loop, according to the International Union of Pure and Applied Chemistry (IUPAC), which is typical of mesoporous structures [44]. The hysteresis loops (Fig. 4) of natural halloysite, calcined, and calcined acid-treated halloysites are observed between 0.5 and 0.9, which is associated with large pore sizes in the samples [45, 47, 48].

The presence of both micropores and macropores is strongly supported by the observation of hysteresis loops at pressures greater than $p/p_0 = 0.5$ (Fig. 4). The isotherms of calcined halloysite nanotubes at 250 ˚C and 600 ˚C showed identical pore size distribution curves (Fig. 4) [45, 47, 48]. Hysteresis loops demonstrate the preservation of mesoporous structure in acid-treated halloysite nanotubes, which was also shown in SEM images (Fig. 2a-f) and pore size distribution curves (Fig. 5).

The pore volume and BET surface area values of natural and calcined acid treated halloysite nanotubes are summarized in Table 1. Up to 600 ˚C, the BET surface area of halloysite remained relatively constant. Additionally, it is possible to see an increase in the mesopore and total volumes of halloysite after acid treatment (Table 1). The acid treatment of halloysite nanotube increases their specific surface area and porosity. As the acid concentration rises, mesopores are further enlarged to become macropores, and this finding is obviously observed [36, 45, 47, 48]. The formation of macropores is indicated by the larger BET surface area and pore volume of the acid-treated halloysite nanotubes. As a result, the acid treatment increases the mesopore volumes of halloysite [36, 43, 45–48].

The average pore size of natural and calcined halloysite nanotubes is range of 11.0–14.0 nm in diameter [45] (Table 1). The pore size distribution curves are multimodal for the studied samples, and the multimodal distribution of the curves demonstrates the presence of large pores in the treated sample [45–48]. For the sample that was calcined at 600 ˚C and has the most surface area, the curve shows more acute peaks. This outcome demonstrates that the treatment with acid at a 2 M concentration may have caused the formation of regular porosity inside the calcined at 600 ˚C halloysite nanotube [46, 47]. The isotherm and pore size distribution curves made it possible to observe an increase in the specific surface areas and pore volumes after the acid treatment process in the calcined halloysite nanotubes.

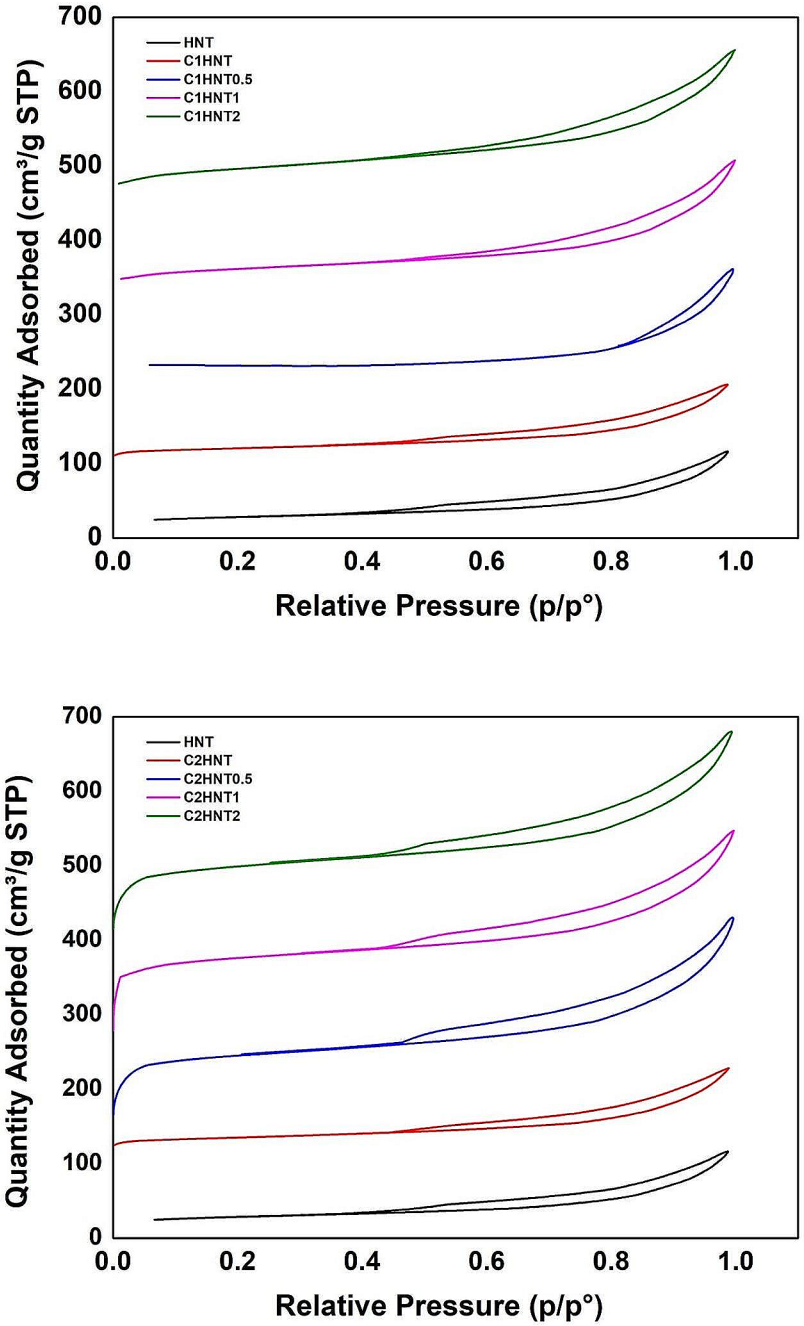


**Fig. 4** Nitrogen adsorption-desorption isotherms of **(a)** HNT, C1HNT, C1HNTC0.5, C1HNT1, C1HNT2, **(b)** HNT, C2HNT, C2HNT0.5, C2HNT1 and C2HNT2

## Differential thermal analysis

Thermogravimetric analysis was carried out to assess the thermal stability of the natural and treated halloysite nanotubes under reaction conditions. When the the DTA and TGA curves of the samples were compared, it was found that the composition and structure of the calcined halloysite nanotube did not significantly change at 250 ˚C but did at 600 ˚C (Fig. 6). The observation that the composition and structure of calcined halloysite nanotubes did not change significantly at 250 ˚C suggests that the material remains relatively stable at this temperature. The first two endothermic peaks seen in the range of 50–300 ˚C in the TGA/DTA curves of natural and acid-treated calcined halloysite nanotubes (Fig. 6) may be caused by the loss of adsorbed and interlayer water [42–44, 46]. At this stage, it is possible to observe that the weight loss is greater for the hydrochloric acid-treated calcined halloysite nanotubes, indicating that

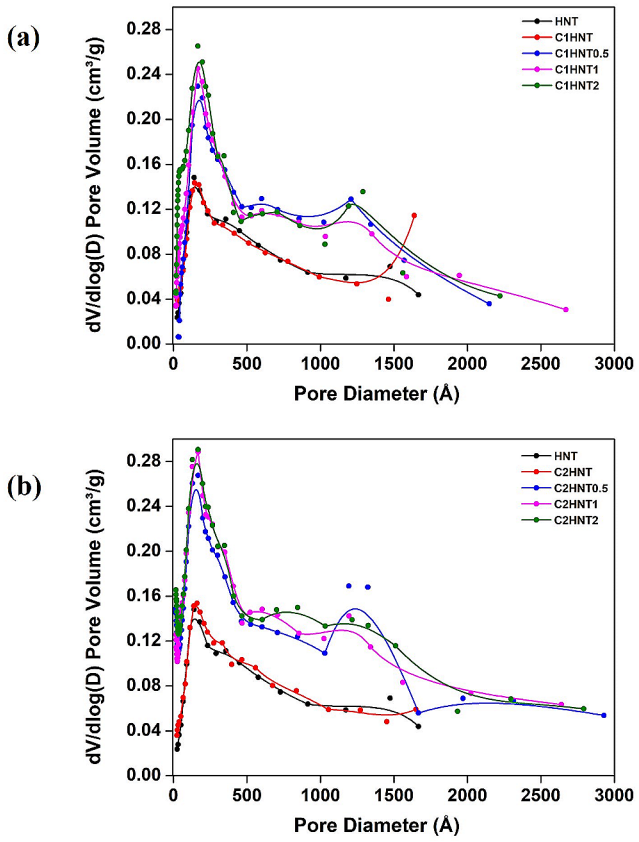


**Fig. 5** Pore size distribution curves of **(a)** HNT, C1HNT, C1HNTC0.5, C1HNT1, C1HNT2, **(b)** HNT, C2HNT, C2HNT0.5, C2HNT1 and C2HNT2

more water has been adsorbed onto these nanotubes as a result of the hydrochloric acid treatment.

This might be because acid treatment increased the amount of surface area, which increased the water adsorption. The second endothermic peak observed between 50 and 300 ˚C may be related to the structural decomposition of halloysite [45, 48, 49]. The halloysite nanotube that was calcined at 600 ˚C did not exhibit the second endothermic peak between 50 and 300 ˚C. It is thought that this may be due to the amorphisation of the structure caused by calcination at 600 ˚C [46]. The increase in acid concentration increased the structural decomposition of halloysite, leading to changes in the endothermic peaks in the treated samples. The TGA curves of the natural, calcined and acid-treated halloysite nanotubes are consistent with the DTA results. When the TGA profiles of the natural and acid-treated calcined halloysite nanotubes were compared, it was found that acid treatment increased the amount of physisorbed water and that it increased with an increase in acid concentration. This is attributed to the possibility that acid treatment increases surface area, as displayed by BET analysis. In addition, the weight loss of acid-treated calcined samples at 600 ˚C is a little higher compared to their counterparts at 250 ˚C. This may be attributed to the dehydroxylation of halloysite during acid treatment after precalcination [46]. In the TGA curves, the weight loss for samples that were calcined at 600 ˚C was clearly discernible as a rapid loss at 200 ˚C, and the other one was observed as a continuous curve between 200 and 800 ˚C. It is possible to observe that the weight loss at the first stage is higher for HNTs calcined at 600 ˚C and treated with hydrochloric acid, which suggests that these HNTs contain more adsorbed water due to their amorphous structure. As it can be seen, acid treatment after precalcination may have a significant impact on how much weight is lost during the thermal analysis. The changes observed at 600 ˚C indicate that this temperature is associated with thermal events leading to dehydroxylation or amorphization of the halloysite nanotubes. The results indicate that calcination at high temperatures and treatment with hydrochloric acid can reduce the degree of crystallisation of halloysite. Halloysite is an aluminosilicate mineral and at elevated temperatures dehydroxylation or amorphization processes may occur. The observed high mass loss may be due to structural changes such as dehydroxylation or amorphisation of the nanotubes. The above results have also been confirmed by XRD, SEM and FT-IR observations. It was also found that there was fairly good agreement between the thermogravimetric and XPS results. The TGA and DTA images of the natural and calcined halloysite nanotubes indicate that the mineral framework was preserved following the thermal treatment (Fig. 6) [36, 37].

**Table 1** Textural properties of samples

| Catalyst (Temperature ˚C) | Surface Area ($m^2/g$) | Pore volume ($cm^3/g$) | Pore diameter (Å) |
|---|---|---|---|
| Natural HNT | 99.3708 | 0.172605 | 139.597 |
| CHNT (250 ˚C) | 53.5105 | 0.153651 | 112.1522 |
| CHNT (600 ˚C) | 53.3572 | 0.158720 | 118.9870 |
| C1HNT0.5 (250 ˚C) | 102.4114 | 0.213919 | 125.034 |
| C1HNT1 (250 ˚C) | 121.9968 | 0.263271 | 111.145 |
| C1HNT2 (250 ˚C) | 160.7061 | 0.302649 | 91.611 |
| C2HNT0.5 (600 ˚C) | 378.4799 | 0.347753 | 95.713 |
| C2HNT1 (600 ˚C) | 384.0613 | 0.331672 | 88.308 |
| C2HNT2 (600 ˚C) | 392.8677 | 0.364051 | 89.693 |

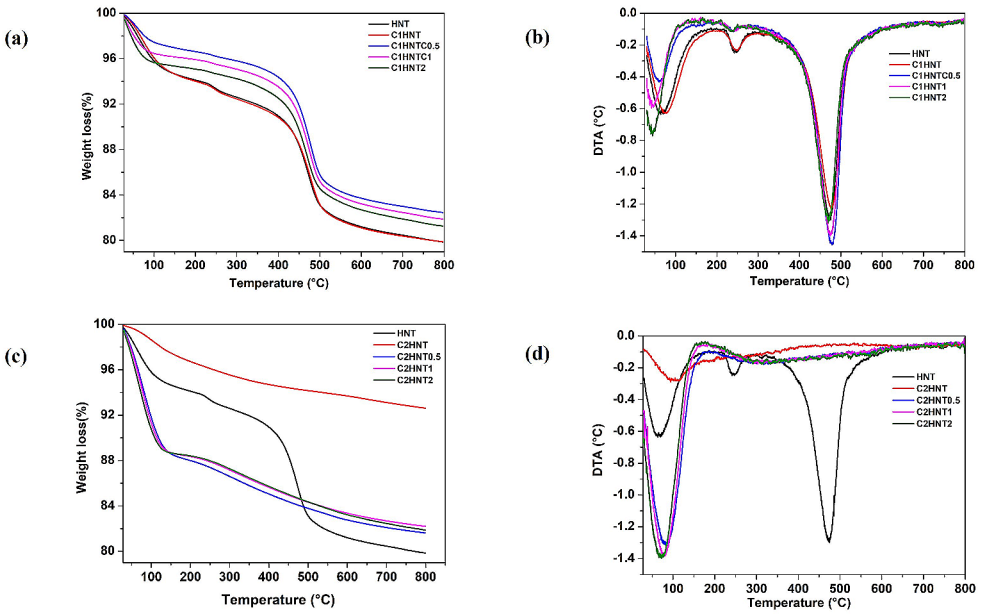


**Fig. 6** **(a)** TGA curves of HNT, C1HNT, C1HNTC0.5, C1HNT1, C1HNT2, **(b)** DTA curves of HNT, C1HNT, C1HNTC0.5, C1HNT1, C1HNT2, **(c)** TGA curves of HNT, C2HNT, C2HNT0.5, C2HNT1 and C2HNT2, **(d)** TGA curves of HNT, C2HNT, C2HNT0.5, C2HNT1 and C2HNT2

## XPS analysis

X-ray photoelectron spectroscopy (XPS) is an important technique used to characterize the surface properties of clay minerals. The influence of treatment with hydrochloric acid on the surfaces of halloysite nanotubes calcinated at two different temperatures was investigated by the XPS method. In the analysis of the XPS spectra of the samples studied, the binding energies of the photoelectron peaks were analysed using the carbon C1s photoelectron peak at 284.6 eV for calibration. A comparison of the XPS spectra of natural halloysite and samples calcined at two different temperatures and activated with hydrochloric acid is shown in Fig. 7. The spectra show that the samples have aluminum (Al), silica (Si), oxygen (O) and carbon (C) elements (Fig. 7). In the XPS spectra of the natural halloysite (Fig. 7), the 2s and 2p bands of Si and Al, as expected depending on the chemical structure of halloysite, were observed in the range of 0-150 eV [53–58]. In agreement with the XRD results no other minerals are present. Furthermore, no impurities were detected in the spectrum presented. As for most of the samples exposed to the atmosphere, a C 1s photoelectron peak with a binding energy of around 284.6 eV was also observed and used as an energy reference for the spectra [54–58].

The XPS spectra of the natural halloysite revealed that the Al 2p, Al 2s, Si 2p, Si 2s and O 2s peaks are positioned in the range of 0-200 eV, which indicates the presence of Al–O and Si–O bonds [56, 58]. The peaks of O 1s observed around 550 eV show the presence of the O–Si and O–Al bonds, which have been expected based on the chemical structure of natural halloysite [56, 58]. In addition, the other peak detected at around 1000 eV in the XPS spectrum of natural halloysite is assigned as the Auger peak (O KLL) [55, 57]. As the main aim of the present study is to investigate the influence of the calcination temperature and acid treatment on the sample's chemical composition, the XPS spectra were also registered for the activated halloysite nanotubes in 2 M acid HCl at 250 and 600 °C (Fig. 7). It was observed from comparing the XPS spectra of the natural halloysite and acid-treated calcined halloysite samples that the intensity of peaks coming from Si and Al had changed (Fig. 7). No substantial changes were observed up to 250 ˚C. A comparison of the binding energies related to different photoelectron peaks with those of natural halloysite shows that calcination at 250 °C produces a similar atomic environment, whereas calcination at 600 °C changes the configuration of the atoms around the environment (Fig. 7). This means that calcination at 600 °C has caused a change in the arrangement of the atoms, suggesting changes in bonding, coordination, or the overall chemical structure of the halloysite material. Especially, the observation of nearly absent XPS peaks from aluminum (Al) in the halloysite nanotube structure at 600 ˚C suggests important information about the structural changes and amorphization of the halloysite sample at elevated temperatures (at 600 ˚C). This result indicates that the crystal structure of the halloysite nanotubes has become amorphous at 600 ˚C, in agreement with the XRD results. However, the changes in the intensity of the XPS peaks originating from aluminum suggest a reduction in the concentration of aluminum on the surface of the halloysite nanotubes at higher temperatures. The results obtained with the XPS analysis show that at 600 ˚C calcination temperatures, the amount of aluminum atoms at the halloysite nanotube surface is significantly reduced. It can be concluded that there is a fairly good agreement at the peak positions for the natural halloysite and the sample

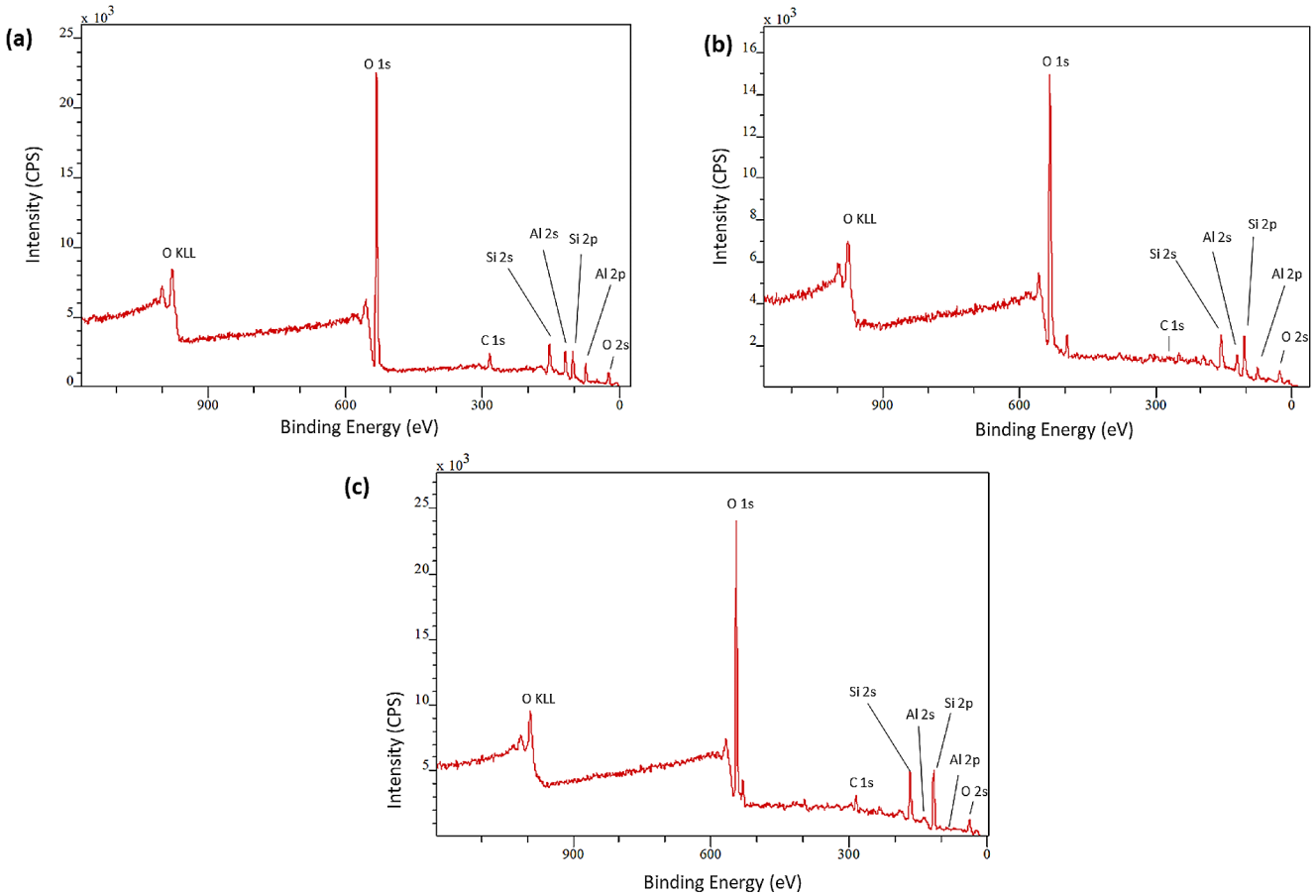


**Fig. 7** XPS spectra of **(a)** HNT, **(b)** C1HNTC2, **(c)** C2HNT2

calcined at 250 °C and then treated with acid. However, as a result of the acid treatment after the sample was calcined at 600 °C, some peaks have gone unobserved. The results of this study are significant for future research on chemical reactions involving halloysite nanotubes because they demonstrate the viability of using the XPS technique to analyze halloysite nanotubes.

## Conclusions

The effects of the acid treatment after precalcination on the structural and chemical properties of halloysite nanotubes have been studied. The obtained results confirm that the acid treatment at the chosen concentrations has helped the tubular structure of the halloysite to retain. This suggests that the halloysite nanotubes can withstand the selected acid treatment conditions, preserving their morphology and integrity. All of the observed XRD peaks for the halloysite samples are consistent with the reported values for halloysite-7 (JCPDS card no. 29-1487). The XRD results indicate that the crystalline structure of halloysite is stable up to 250 ˚C but becomes the amorphization of the structure at 600 ˚C. The XPS results of the calcined and acid-treated halloysite nanotubes at 600 ˚C confirm the structure's amorphization. The results of the XPS method confirm that the calcination temperature applied before acid treatment of the halloysite samples significantly affects the changes in the structure of the halloysite samples, which were also confirmed in the XRD analysis. The acid treatment after precalcination not only preserved the tubular structure but also allowed for an increase in the size of the specific surface area and volume of the adsorption pores, as demonstrated in SEM and nitrogen adsorption-desorption analyses. The FT-IR spectra show that acid treatments after calcination have no important influence on the characteristic absorption bands of halloysite and may be preserved in nanotubular structure. The nitrogen adsorption-desorption and pore size distribution analyses of the samples reveal that acid treatment increases surface area and pore volume. It was possible to see that acid treatment increased the surface area and pore volume of halloysite nanotubes. According to the TGA and DTA analyses, acid treatment increased the amount of adsorbed water and that amount increased in direct proportion to the acid concentration. It is thought that this further confirms the increase in surface area caused by acid treatment. As a

result, it is believed that the acid-treated halloysite nanotubes may be a useful adsorbent that is inexpensive.

**Funding** This research did not receive any specific grant from funding agencies in the public, commercial, or not-for-profit sectors. Open access funding provided by the Scientific and Technological Research Council of Türkiye (TÜBİTAK).
Open access funding provided by the Scientific and Technological Research Council of Türkiye (TÜBİTAK).

**Data availability** All data are contained within the article.

## Declarations

**Compliance with ethical standards / Competing interests** The author declare that they have no competing interests.



## References

1. Bordeepong, S., Bhongsuwan, D., Pungrassami, T., Bhongsuwan, T.: Characterization of halloysite from Thung Yai district, Nakhon Si Thammarat Province, in Southern Thailand. Songklanakarin J. Sci. Technol. **33**, 599–607 (2011)
2. Yuan, P., Tan, D., Annabi-Bergaya, F.: Properties and applications of halloysite nanotubes: Recent research advances and future prospects. Appl. Clay Sci. **112–113**, 75–93 (2015). https://doi.org/10.1016/j.clay.2015.05.001
3. Papoulis, D.: Progressive formation of halloysite from the hydrothermal alteration of biotite and the formation mechanisms of anatase in altered volcanic rocks from limnos island, northeast aegean sea, greece. 57, 566–577 (2009). https://doi.org/10.1346/CCMN.2009.0570505
4. Joussein, E., Petit, S., Churchman, J., Theng, B., Righi, D., Delvaux, B.: Halloysite clay minerals – a review. Clay Miner. **40**, 383–426 (2005). https://doi.org/10.1180/0009855054040180
5. Zhang, Y., Tang, A., Yang, H., Ouyang, J.: Applications and interfaces of halloysite nanocomposites. Appl. Clay Sci. **119**, 8–17 (2016). https://doi.org/10.1016/j.clay.2015.06.034
6. Tarì, G., Bobos, I., Gomes, C.S.F., Ferreira, J.M.F.: Modification of Surface Charge Properties during Kaolinite to Halloysite-7Å Transformation. J. Colloid Interface Sci. **210**, 360–366 (1999). https://doi.org/10.1006/jcis.1998.5917
7. Yang, H., Zhang, Y., Ouyang, J.: Physicochemical Properties of Halloysite. Elsevier Ltd (2016). https://doi.org/10.1016/B978-0-08-100293-3.00004-2
8. Liu, M., Jia, Z., Jia, D., Zhou, C.: Recent advance in research on halloysite nanotubes-polymer nanocomposite. Prog. Polym. Sci. **39**, 1498–1525 (2014). https://doi.org/10.1016/j.progpolymsci.2014.04.004
9. Churchman, G.J., Davy, T.J., Aylmore, L.A.G., Gilkes, R.J., Self, P.G.: Characteristics of fine pores in some Halloysites. Clay Miner. **30**, 89–98 (1995). https://doi.org/10.1180/claymin.1995.030.2.01
10. Yousefi, P., Hamedi, S., Garmaroody, E.R., Koosha, M.: Antibacterial nanobiocomposite based on halloysite nanotubes and extracted xylan from bagasse pith. Int. J. Biol. Macromol. **160**, 276–287 (2020). https://doi.org/10.1016/j.ijbiomac.2020.05.209
11. Wang, L.-F., Rhim, J.-W.: Functionalization of halloysite nanotubes for the preparation of carboxymethyl cellulose-based nanocomposite films. Appl. Clay Sci. **150**, 138–146 (2017). https://doi.org/10.1016/j.clay.2017.09.023
12. Stavitskaya, A., Shakhbazova, C., Cherednichenko, Y., Nigamatzyanova, L., Fakhrullina, G., Khaertdinov, N., Kuralbayeva, G., Filimonova, A., Vinokurov, V., Fakhrullin, R.: Antibacterial properties and in vivo studies of tannic acid-stabilized silver–halloysite nanomaterials. Clay Miner. **55**, 112–119 (2020). https://doi.org/10.1180/clm.2020.17
13. Ghalei, S., Hopkins, S., Douglass, M., Garren, M., Mondal, A., Handa, H.: Nitric oxide releasing halloysite nanotubes for biomedical applications. J. Colloid Interface Sci. **590**, 277–289 (2021). https://doi.org/10.1016/j.jcis.2021.01.047
14. Vikulina, A., Voronin, D., Fakhrullin, R., Vinokurov, V., Volodkin, D.: Naturally derived nano- and micro-drug delivery vehicles: Halloysite, vaterite and nanocellulose. New J. Chem. **44**, 5638–5655 (2020). https://doi.org/10.1039/C9NJ06470B
15. Zargarian, S.S., Haddadi-Asl, V., Hematpour, H.: Carboxylic acid functionalization of halloysite nanotubes for sustained release of diphenhydramine hydrochloride. J. Nanopart. Res. **17**, 1–13 (2015). https://doi.org/10.1007/s11051-015-3032-3
16. Levis, S.R., Deasy, P.B.: Characterisation of halloysite for use as a microtubular drug delivery system. Int. J. Pharm. **243**, 125–134 (2002). https://doi.org/10.1016/S0378-5173(02)00274-0
17. Li, W., Liu, D., Zhang, H., Correia, A., Mäkilä, E., Salonen, J., Hirvonen, J., Santos, H.A.: Microfluidic assembly of a nano-in-micro dual drug delivery platform composed of halloysite nanotubes and a pH-responsive polymer for colon cancer therapy. Acta Biomater. **48**, 238–246 (2017). https://doi.org/10.1016/j.actbio.2016.10.042
18. Mo, X., Wu, F., Li, Y., Cai, X.: Hyaluronic acid-functionalized halloysite nanotubes for targeted drug delivery to CD44-overexpressing cancer cells. Mater. Today Commun. **28**, 102682 (2021). https://doi.org/10.1016/j.mtcomm.2021.102682
19. Persano, F., Gigli, G., Leporatti, S.: Halloysite-based nanosystems for Biomedical Applications. Clays Clay Miner. (2021). https://doi.org/10.1007/s42860-021-00135-8
20. Danyliuk, N., Tomaszewska, J., Tatarchuk, T.: Halloysite nanotubes and halloysite-based composites for environmental and biomedical applications. J. Mol. Liq. **309**, 113077 (2020). https://doi.org/10.1016/j.molliq.2020.113077
21. Prinz Setter, O., Movsowitz, A., Goldberg, S., Segal, E.: Antibody-functionalized Halloysite nanotubes for Targeting Bacterial cells. ACS Appl. Bio Mater. **4**, 4094–4104 (2021). https://doi.org/10.1021/acsabm.0c01332
22. Yang, C., Liu, P., Zhao, Y.: Preparation and characterization of coaxial halloysite/polypyrrole tubular nanocomposites for electrochemical energy storage. Electrochim. Acta. **55**, 6857–6864 (2010). https://doi.org/10.1016/j.electacta.2010.05.080
23. Wang, Y., Wang, X., Ye, H., Han, K.: Carbon coated halloysite nanotubes as efficient sulfur host materials for lithium sulfur batteries. Appl. Clay Sci. **179**, 105172 (2019). https://doi.org/10.1016/j.clay.2019.105172
24. Cao, X., Sun, Y., Sun, Y., Xie, D., Li, H., Liu, M.: Conductive halloysite clay nanotubes for high performance sodium ion

battery cathode. Appl. Clay Sci. **213**, 106265 (2021). https://doi.org/10.1016/j.clay.2021.106265
25. Li, Y., Zhou, J., Liu, Y., Tang, J., Tang, W.: Hierarchical nickel Sulfide Coated Halloysite nanotubes for efficient Energy Storage. Electrochim. Acta. **245**, 51–58 (2017). https://doi.org/10.1016/j.electacta.2017.05.140
26. Zhao, M., Liu, P.: Adsorption behavior of methylene blue on halloysite nanotubes. Microporous Mesoporous Mater. **112**, 419–424 (2008). https://doi.org/10.1016/j.micromeso.2007.10.018
27. Ramadass, K., Singh, G., Lakhi, K.S., Benzigar, M.R., Yang, J.H., Kim, S., Almajid, A.M., Belperio, T., Vinu, A.: Halloysite nanotubes: Novel and eco-friendly adsorbents for high-pressure CO2 capture. Microporous Mesoporous Mater. **277**, 229–236 (2019). https://doi.org/10.1016/j.micromeso.2018.10.035
28. Inagaki, M., Kondo, N., Nonaka, R., Ito, E., Toyoda, M., Sogabe, K., Tsumura, T.: Structure and photoactivity of titania derived from nanotubes and nanofibers. J. Hazard. Mater. **161**, 1514–1521 (2009). https://doi.org/10.1016/j.jhazmat.2008.05.003
29. Li, L., Wang, F., Lv, Y., Liu, J., Zhang, D., Shao, Z.: Halloysite nanotubes and Fe3O4 nanoparticles enhanced adsorption removal of heavy metal using electrospun membranes. Appl. Clay Sci. **161**, 225–234 (2018). https://doi.org/10.1016/j.clay.2018.04.002
30. Gupta, V.K., Ali, I., Saini, V.K.: Adsorption studies on the removal of Vertigo Blue 49 and Orange DNA13 from aqueous solutions using carbon slurry developed from a waste material. J. Colloid Interface Sci. **315**, 87–93 (2007). https://doi.org/10.1016/j.jcis.2007.06.063
31. Liu, R., Zhang, B., Mei, D., Zhang, H., Liu, J.: Adsorption of methyl violet from aqueous solution by halloysite nanotubes. Desalination. **268**, 111–116 (2011). https://doi.org/10.1016/j.desal.2010.10.006
32. Zhao, Y., Abdullayev, E., Vasiliev, A., Lvov, Y.: Halloysite nanotubule clay for efficient water purification. J. Colloid Interface Sci. **406**, 121–129 (2013). https://doi.org/10.1016/j.jcis.2013.05.072
33. Duan, Z., Zhao, Q., Wang, S., Huang, Q., Yuan, Z., Zhang, Y., Jiang, Y., Tai, H.: Halloysite nanotubes: Natural, environmental-friendly and low-cost nanomaterials for high-performance humidity sensor. Sens. Actuators B: Chem. **317**, 128204 (2020). https://doi.org/10.1016/j.snb.2020.128204
34. Liu, M., Zhang, Y., Zhou, C.: Nanocomposites of halloysite and polylactide. Appl. Clay Sci. **75–76**, 52–59 (2013). https://doi.org/10.1016/j.clay.2013.02.019
35. Jeamjumnunja, K., Cheycharoen, O., Phongzitthiganna, N., Hannongbua, S., Prasittichai, C.: Surface-modified Halloysite nanotubes as Electrochemical CO2Sensors. ACS Appl. Nano Mater. **4**, 3686–3695 (2021). https://doi.org/10.1021/acsanm.1c00174
36. Zhang, A.B., Pan, L., Zhang, H.Y., Liu, S.T., Ye, Y., Xia, M.S., Chen, X.G.: Effects of acid treatment on the physico-chemical and pore characteristics of halloysite. Colloids Surf., a. **396**, 182–188 (2012). https://doi.org/10.1016/j.colsurfa.2011.12.067
37. Zhang, Y., Li, Y., Zhang, Y., Ding, D., Wang, L., Liu, M., Zhang, F.: Thermal behavior and kinetic analysis of halloysite–stearic acid complex. J. Therm. Anal. Calorim. **135**, 2429–2436 (2019). https://doi.org/10.1007/s10973-018-7354-0
38. Mahajan, A., Gupta, P.: Halloysite nanotubes based heterogeneous solid acid catalysts. New J. Chem. **44**, 12897–12908 (2020). https://doi.org/10.1039/d0nj02846k
39. Surya, I., Masa, A., Ismail, H., Hayeemasae, N.: Acid-treated halloysite nanotubes filled natural rubber composites. IOP Conference Series: Materials Science and Engineering. 801, 012087 (2020). https://doi.org/10.1088/1757-899X/801/1/012087
40. Gaaz, T.S., Sulong, A.B., Kadhum, A.A.H., Nassir, M.H., Al-Amiery, A.A.: Impact of sulfuric acid treatment of halloysite on physico-chemic property modification. Materials. **9** (2016). https://doi.org/10.3390/ma9080620
41. Lenarda, M., Storaro, L., Talon, A., Moretti, E., Riello, P.: Solid acid catalysts from clays: Preparation of mesoporous catalysts by chemical activation of metakaolin under acid conditions. J. Colloid Interface Sci. **311**, 537–543 (2007). https://doi.org/10.1016/j.jcis.2007.03.015
42. Belver, C., Bañares Muñoz, M.A., Vicente, M.A.: Chemical activation of a kaolinite under acid and alkaline conditions. Chem. Mater. **14**, 2033–2043 (2002). https://doi.org/10.1021/cm0111736
43. Garcia-Garcia, D., Ferri, J.M., Ripoll, L., Hidalgo, M., Lopez-Martinez, J., Balart, R.: Characterization of selectively etched halloysite nanotubes by acid treatment. Appl. Surf. Sci. **422**, 616–625 (2017). https://doi.org/10.1016/j.apsusc.2017.06.104
44. Jin, J., Zhang, Y., Ouyang, J., Yang, H.: Halloysite nanotubes as hydrogen storage materials. Phys. Chem. Miner. **41**, 323–331 (2014). https://doi.org/10.1007/s00269-013-0651-z
45. Yuan, P., Tan, D., Annabi-Bergaya, F., Yan, W., Fan, M., Liu, D., He, H.: Changes in structure, morphology, porosity, and surface activity of mesoporous halloysite nanotubes under heating. Respir. Care. **58**, 561–573 (2013). https://doi.org/10.1346/CCMN.2012.0600602
46. Belkassa, K., Bessaha, F., Marouf-Khelifa, K., Batonneau-Gener, I., Comparot, J., Khelifa, A.: Physicochemical and adsorptive properties of a heat-treated and acid-leached Algerian halloysite. Colloids Surf., a. **421**, 26–33 (2013). https://doi.org/10.1016/j.colsurfa.2012.12.048
47. Deng, L., Yuan, P., Liu, D., Du, P., Zhou, J., Wei, Y., Song, Y., Liu, Y.: Effects of calcination and acid treatment on improving benzene adsorption performance of halloysite. Appl. Clay Sci. **181**, 105240 (2019). https://doi.org/10.1016/j.clay.2019.105240
48. Kadi, S., Lellou, S., Marouf-Khelifa, K., Schott, J., Gener-Batonneau, I., Khelifa, A.: Preparation, characterisation and application of thermally treated Algerian halloysite. Microporous Mesoporous Mater. **158**, 47–54 (2012). https://doi.org/10.1016/j.micromeso.2012.03.014
49. Saklar, S., Yorukoglu, A.: Effects of hydrochloric acid leaching on ilmenite. **1**, 1–10 (2015). https://doi.org/10.5277/ppmp150108
50. Rubel, M.H.K., Hossain, M.E., Parvez, M.S., Rahaman, M.M., Islam, M.S., Kumada, N., Kojima, S.: Low-temperature synthesis of potassium triniobate (KNb3O8) ceramic powder by a novel aqueous organic gel route. J. Aust. Ceram. Soc. **55**, 759–764 (2019). https://doi.org/10.1007/s41779-018-0287-z
51. Rashid, M.A., Islam, M.M., Abu, M., Saiham, A., Ahsan, M.R., Mortuza, M.G., Rubel, M.H.K.: Spectroscopic Study of xSiO2 (1-x)Sb2O3 for x = 10%, 20%, 30%, 40% and 50% mol% as Quench Glass and Glass ceramics. J. Sci. Eng. Res. **6**, 144–152 (2019)
52. Islam, M.M., Rashid, M.A., Ahamed, M.P., Hossain, M.E., Ahsan, M.R., Mortuza, M.G., Rubel, M.H.K.: Morphogenesis of Silicovanadate glasses: Investigation of Physical Properties. J. Eng. Advancements. **02**, 16–24 (2021). https://doi.org/10.38032/jea.2021.02.003
53. Kloprogge, J.T.: Characterisation of Halloysite by Spectroscopy. Elsevier Ltd (2016). https://doi.org/10.1016/B978-0-08-100293-3.00006-6
54. Szczepanik, B., Banaś, D., Kubala-Kukuś, A., Szary, K., Słomkiewicz, P., Rędzia, N., Frydel, L.: Surface properties of halloysite-carbon nanocomposites and their application for adsorption of Paracetamol. Materials. **13**, 1–17 (2020). https://doi.org/10.3390/ma13245647
55. Szczepanik, B., Słomkiewicz, P., Garnuszek, M., Rogala, P., Banaś, D., Kubala-Kukuś, A., Stabrawa, I.: Effect of temperature on halloysite acid treatment for efficient chloroaniline removal from aqueous solutions. Clays Clay Miner. **65**, 155–167 (2017). https://doi.org/10.1346/CCMN.2017.064056

56. Al-Gaashani, R., Zakaria, Y., Gladich, I., Kochkodan, V., Lawler, J.: XPS, structural and antimicrobial studies of novel functionalized halloysite nanotubes. Sci. Rep. **12**, 1–15 (2022). https://doi.org/10.1038/s41598-022-25270-7
57. Kubala-Kukuś, A., Szczepanik, B., Stabrawa, I., Banaś, D., Szary, K., Pajek, M., Rogala, P., Wójtowicz, K., Słomkiewicz, P.: X-ray photoelectron spectroscopy analysis of chemically modified halloysite. Radiat. Phys. Chem. **175**, 108149 (2020). https://doi.org/10.1016/j.radphyschem.2019.02.008
58. Kloproagea, T., Woodb, B.J.: Chemıcal Structures Of The AI, Si, O, (OH), BY X-Ray Photoelectron Spectroscopy ofeueensland Bondıng (Table (2015)